Pacific Graphics (2016)
E. Grinspun, B. Bickel, and Y. Dobashi (Editors)

Short Paper

Dynamic Skin Deformation Simulation Using Musculoskeletal Model and Soft Tissue Dynamics

A. Murai[1], Q. Y. Hong[2], K. Yamane[3], and J. K. Hodgins[3]

[1]National Institute of Advanced Industrial Science and Technology, [2]Carnegie Mellon University, [3]Disney Research

Abstract

Deformation of skin and muscle is essential for bringing an animated character to life. This deformation is difficult to animate in a realistic fashion using traditional techniques because of the subtlety of the skin deformations that must move appropriately for the character design. In this paper, we present an algorithm that generates natural, dynamic, and detailed skin deformation (movement and jiggle) from joint angle data sequences. The algorithm consists of two steps: identification of parameters for a quasi-static muscle model using a musculoskeletal model and a short sequence of skin deformation data, and simulation of dynamic muscle and soft tissue deformation with quasi-static muscle shape and a mass-spring-damper system. We demonstrate our method using skeletal motion capture data of a subject (whose data is not used for training) to create appropriate skin deformations for muscle co-contraction and external impacts. Experimental results show that the simulated skin deformations are quantitatively and qualitatively similar to the measured actual skin deformations.

Categories and Subject Descriptors (according to ACM CCS): I.3.7 [Computer Graphics]: Three-Dimensional Graphics and Realism—Animation

1. Introduction

Skin deformation of animated characters must be natural, dynamic, and detailed if the characters are to appear realistic and lifelike. This level of realism is particularly important in scenes of rich natural environments such as those in *The Jungle Book* and realistic special-effect shots such as those in *Planet of the Apes*. These deformations are essential for creating a sense of life: tension in the muscles and jiggle of the underlying muscle and soft tissue convey the exertion of the character and the dynamics of the motion. A number of algorithms have been created for generating plausible skin deformation [LAR*14]. Recently, more effort has been expended in making anatomical models [SLST14].

In this paper, we present an algorithm that generates detailed skin deformation (movement and jiggle) from a skeleton animation based on standard motion capture joint angle data and three models: 1) a quasi-static muscle model, 2) a muscle dynamics model, and 3) a soft tissue dynamics model. Our approach consists of two main steps: identification of quasi-static muscle model parameters followed by simulation of dynamic skin deformation. In the identification step, which is performed only once for each body type, we compute subject-specific muscle shape parameters using a musculoskeletal model [MTMN14] and a short sequence of skin deformation data captured with a dense marker set from [PH08]. The quasi-static muscle model relates the quasi-static muscle shape to muscle length and tension, which can be obtained by computing the inverse kinematics and dynamics using a musculoskeletal model and joint angle data. Once a muscle deformation model is obtained, we can simulate the dynamic muscle deformations using only joint angle data. These can be obtained from skeletal motion capture (50-60 markers) or from a physically plausible keyframe animation. The simulation step first uses the quasi-static muscle deformation model identified in the previous step to obtain the quasi-static muscle shape for the given motion sequence. It then computes the dynamic skin deformation by simulating the passive muscle and soft tissue dynamics modeled as a mass-spring-damper system.

We realize simulation of detailed skin deformation that has anatomical and physical consistency, while maintaining manageable user and computational complexity. The contributions of our work include: 1) A method for identifying muscle deformation model parameters from a short sequence of skin deformation data measured by motion capture using a dense marker set (400–450 markers), 2) A method for applying the muscle and skin deformation model to joint angle data recorded with 50-60 markers to create new sequences with detailed skin and muscle deformation. Our approach realizes a good balance between computational cost and accuracy by applying a parametric model for muscle deformation and a simple spring-damper model for soft tissue simulation.

2. Related Work

Skin deformation and dynamics are required for a realistic and natural-looking character, and therefore many approaches have

DOI: 10.2312/pg.20161335

been developed to generate this motion. One of the most common approaches is linear-blend skinning in which each skin vertex position is computed using a weighted sum of the positions of nearby joints. However, the skin often lacks realism because of artifacts and because small scale details in the skin deformation are missing with linear-blend skinning. A number of algorithms have been created to overcome these problems [LAR*14].

More realistic models fall into two broad classes: simulated and data-driven. To model human-like creatures, researchers have proposed a layered approach in which the skin is driven by interactions between multiple underlying layers with different properties that are based on anatomy [LGK*12]. Various parts of the human body have been modeled in detail, such as face [LAR*14]. With this approach, the research focus has been on modeling the shape and deformation of muscles to reduce artifacts and express details in skin deformation. Deformation of muscles and soft tissues is often simulated by physics-based models such as mass-spring-damper models [ZCCD04] and volumetric models such as the finite element method (FEM) [KMF*96, BTS*05] or the finite volume method [FLP14]. To avoid issues with stability, data-driven approaches model skin deformation directly from data rather than simulating the behavior of each layer in the musculoskeletal structure. Anguelov and colleagues [ASK*05] used SCAPE to build a pose deformation model. Park and Hodgins used motion capture to collect data, and then trained the parameters of a mass-spring model from the captured data [PH08]. Their mass-spring model treated the body parts as a homogeneous medium rather than having separate models for muscles, fat, and interstitial tissue as we do.

In biomechanics and robotics, many musculoskeletal models have been developed for simulation and analysis of human body dynamics [DAA*07, MTMN14]. However, these models focus on accurate simulation and analysis of human motion and do not include computation of the skin or muscle shape as is needed for animated characters.

3. Method

During dynamic motion, actuated muscles cause bone motion as well as bulging due to tension and length changes. Additionally, muscles and soft tissue, including skin, fat, and viscera, deform passively in response to the bone and muscle movement as well as external forces from the environment. Accordingly, our skin deformation model consists of three sub-models (Figure 1 lower left):

1. A quasi-static muscle model that relates the muscle length and tension to the quasi-static muscle shape. This model represents the muscle bulging and relaxation at different activation levels.
2. A muscle dynamics model that describes the passive dynamics of muscles using a mass-spring-damper system. The model consists of point masses placed at the vertices of the muscle polygon model and connected by springs and dampers. Each point mass is also connected to the corresponding vertex of the quasi-static muscle by a spring and damper.
3. A soft tissue dynamics model that describes the passive dynamics of the skin and subcutaneous fat using a mass-spring-damper system. The model consists of point masses placed at the vertices of the polygons on the skin surface with springs and dampers connecting them to neighboring vertices and to the point masses on the dynamic muscle or bone surfaces.

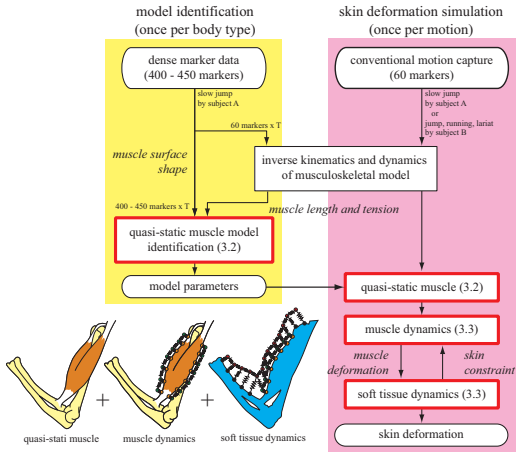

Figure 1: *Three models used in our skin deformation model (lower left), and block diagram of the identification and simulation processes.*

Figure 1 shows the block diagrams of the identification and simulation processes, where the blocks with red borders are the new components developed in this work. The details are explained in the following subsections. In Section 3.1, we review the skin deformation data collection process and the musculoskeletal model. We then present the quasi-static muscle model and the parameter identification process in Section 3.2. In Section 3.3, we describe the algorithm to simulate the dynamic skin deformation using the muscle and soft tissue dynamics models.

3.1. Skin Deformation Data and Musculoskeletal Model

Identifying the quasi-static muscle model parameters requires sample skin deformation data. We use the data recorded by Park and Hodgins [PH08] using an optical motion capture system with 400–450 reflective markers. For identifying the quasi-static muscle model parameters, we use a slow jump motion that is approximately 300 frames (2.5 seconds) in length. We intentionally select a slow sequence in which the soft tissue dynamics does not play a big role in the skin deformation. In order to obtain the input data for the quasi-static muscle model, we apply the inverse kinematics and dynamics algorithms of a musculoskeletal model [MTMN14] using the trajectories of 60 markers manually chosen from the full set of 400–450 based on the improved version of the Helen Hayes Hospital marker set. The musculoskeletal model used in our work consists of skeleton and musculo-tendon network models. Each of the muscles, tendons, and ligaments is represented by two end points (origin and insertion points), any number of via points, and straight pathways between them. Each origin, insertion, or via point is fixed with respect to a bone, and their locations are computed by solving the forward kinematics (Figure 2).

We first obtain the joint angles of the skeleton model at each frame with an iterative inverse kinematics algorithm using the positions of the 60 markers as soft constraints. Then, the joint torques

required to execute the measured motion are computed by applying a recursive inverse dynamics algorithm for articulated rigid bodies [LWP80]. Finally, we compute the muscle tensions required to produce the joint torques [MTMN14]. The number of muscles is much larger than the number of joint torques and this redundancy is resolved with mathematical optimization. If electromyograph (EMG) data are recorded at the same time, we can obtain physiologically plausible muscle tensions for actions that are not observable from the motion, such as co-contraction [YFN05].

3.2. Modeling and Identification of Quasi-static Muscle Model

We next develop a quasi-static muscle model that computes the quasi-static muscle shape from the muscle length and tension. We first choose about 300 surface muscles from 989 muscles in [MTMN14] because we cannot identify the parameters of the inner muscles from surface data. The remaining 700 muscles are still used for inverse dynamics because their tensions affect the tensions of the surface muscles. We construct the following quasi-static muscle model around the pathway of these 300 muscles.

Because most skeletal muscles have spindle-like shapes, we approximate the quasi-static muscle surface with a spindle whose cross-section perpendicular to the pathway is an ellipse, the size of which varies along the pathway according to a sigmoid function (Figure 2). The pennate muscles such as Pectoralis Major, whose cross sectional shapes are quite different from the ellipsoid shape, are modeled with multiple thin spindle-shaped wires. The sigmoid parameters and the eccentricity are represented as functions of the muscle length and tension. In addition, we divide some muscles at a center point into two parts with different sets of sigmoid function parameters to represent asymmetric muscles such as the Soleus. The same identification and simulation method can be applied to any muscle shape if the pathway of the muscle is given. In the following equations, we omit the muscle index for clarity. We represent the quasi-static muscle surface shape in a cylindrical polar coordinate system for each part whose longitudinal axis is the muscle pathway (Figure 2). For a point on the m-th $(m = 1,2)$ part of a muscle, the distance from the pathway, r_m, is described by the location along the pathway x, the angle from the polar axis θ, and the current frame number t $(t = 1,2,\ldots,T)$ as

$$r_m(x,\theta,t) = \left(\frac{k_{m,3}(t)}{1+e^{k_{m,1}(t)-k_{m,2}(t)x}} + k_{m,4}(t) \right) \times \sqrt{1-\varepsilon^2(t)\sin^2\theta} \quad (1)$$

where sigmoid function parameters $k_{m,n}(t)$ $(m = 1,2,\ n = 1,2,3,4)$ and the eccentricity $\varepsilon(t)$ are functions of the muscle length $l(t)$ and tension $\tau(t)$:

$$k_{m,n}(t) = \alpha_{m,n} l(t) + \beta_{m,n}\tau(t) + \gamma_{m,n} \quad (n = 1,2,3,4) \quad (2)$$

$$\varepsilon(t) = \alpha_5 l(t) + \beta_5 \tau(t) + \gamma_5. \quad (3)$$

In our implementation, the x axis is normalized for each part so that $x = 0$ represents the origin or insertion of a muscle and $x = 1$ represents the center point. The local coordinate system of each part is defined with respect to the closest bone's local coordinate system at the initial skeleton posture. Therefore the local coordinate system does not change discontinuously as long as the skeleton motion is continuous. In this model, the total number of parameters to identify is 27 $(\alpha_{m,n}, \beta_{m,n}, \gamma_{m,n}\ (m = 1,2, n = 1,2,3,4),\ \alpha_5, \beta_5, \gamma_5)$ for each muscle. We determine these parameters at each muscle independently so that the muscle shape fits the skin deformation around the muscle during the motion capture sequence.

Let us define a muscle *segment* as a section of a muscle between two neighboring origin, insertion or via points along the pathway and denote the number of segments in a muscle by L. At each motion capture frame t, we find a user-defined number of markers closest to the pathway that belongs to each segment and represent their positions in the local cylindrical polar coordinate system of the muscle as $\left(\hat{r}_{k,t}, \hat{\theta}_{k,t}, \hat{x}_{k,t}\right)$ $(k = 1,2,\ldots L)$. We then solve an optimization problem to adjust the model parameters so that the total distance between the muscle surface and the positions of the closest markers is minimized. We used a gradient-based algorithm to minimize the following quadratic cost function:

$$Z = \frac{1}{2}\left(Z_r + a_v Z_v + a_t Z_t\right) \quad (4)$$

where a_* are user-defined positive weights. Z_r represents the total squared distance between the muscle surface and measured marker data and is formulated as

$$Z_r = \sum_{t=1}^{T}\sum_{k=1}^{L} \Delta r_{k,t}^T \Delta r_{k,t} \quad (5)$$

$$\Delta r_{k,t} = \hat{r}_{k,t} - \left(r_m(\hat{x}_{k,t}, \hat{\theta}_{k,t}, t) + r_f\right) \quad (6)$$

where m represents the part containing segment k and r_f is a manually chosen fat thickness. We use $r_f = 0.00\,\mathrm{m}$ in the experiment. Z_v represents the variance of the muscle volume across the entire motion sequence and can be formulated by

$$Z_v = \sum_{t=1}^{T}\left(V_1(t) + V_2(t) - \frac{1}{T}\sum_{t=1}^{T}\left(V_1(t) + V_2(t)\right)\right)^2 \quad (7)$$

where $V_m(t)$ is the volume of part m at frame t computed by

$$V_m(t) = l_i(t)\int_0^1 r_m^2(x,0,t)\pi\sqrt{1-\varepsilon^2(t)}dx \quad (8)$$

This term is added to represent the conservation of muscle volume [Kar90]. Z_t is added to constrain the radius at origin, insertion, and center so that the muscle is smoothly connected to the tendons at the ends and to each other at the center. Z_t is formulated as:

$$Z_t = \sum_{t=1}^{T}\left((w - r_1(0,0,t))^2 + (w - r_2(0,0,t))^2 + (r_1(1,0,t) - r_2(1,0,t))^2\right) \quad . \quad (9)$$

where w is a manually chosen tendon radius. We use $w = 0.01\,\mathrm{m}$ in the experiments. We set the weights for Eq. (9) (a_t) high so that the muscle shape is smooth after the optimization $(a_v = 10^0, a_t = 10^2)$.

3.3. Muscle and Soft Tissue Dynamic Deformation

Once the quasi-static muscle model parameters are identified, we use the same set of parameters to simulate the dynamics deformation of the muscles and the soft tissue for new joint angle data sequences. Here, the shape of the quasi-static muscle model defines the rest shape of the dynamic muscle model from its length and tension. We model the bones, the quasi-static muscles, the dynamic muscle, and the skin surface as polygonal surfaces. Let $\mathcal{P}^s$ denote

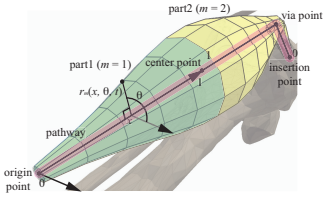

Figure 2: *Muscle shape and its local coordinate system. The red line represents the muscle pathway that connects the origin point, one or more via points, and the insertion point.*

the set of skin vertices, $\mathcal{P}^{qm}$ the vertices on the quasi-static muscle surfaces, $\mathcal{P}^{dm}$ the vertices on the dynamic muscle surfaces, and $\mathcal{P}^{b}$ the vertices on the bone surfaces. In the soft tissue dynamics model (Figure 3, left), each skin vertex $p_s \in \mathcal{P}^{s}$ is connected to:

1. the adjacent skin vertices,
2. a set of nearby muscle vertices, which includes the vertices within the hemisphere whose center is at p_s and radius is $\alpha + r$ (here, $\alpha = 2.0\,\mathrm{cm}$), where r is the distance between p_s and its nearest vertex in $\mathcal{P}^{dm} \cup \mathcal{P}^{b}$ and $\alpha(> 0)$ is the offset, and
3. the bone vertices included in the hemisphere defined above.

Note that a skin vertex may be connected to multiple muscles. These connections allow the skin to slide over the muscle surface to the extent allowed by the spring stiffness. In the muscle dynamics model (Figure 3, right), each muscle vertex $p_{dm} \in \mathcal{P}^{dm}$ is connected to:

1. the adjacent dynamic muscle vertices,
2. the skin vertices that have been connected to p_{dm}, and
3. the corresponding quasi-static muscle vertex p_{qm}.

As a result, the muscle deforms not only because of the skeleton motion but also based on the change in the quasi-static muscle shape due to muscle activation.

If p_i is connected to p_j via a spring and damper pair, the force applied to vertex p_i from p_j, f_{ij}, is computed by

$$f_{ij} = k_{ij}(||x_{ij}|| - l_{ij})\frac{x_{ij}}{||x_{ij}||} + c_{ij}\frac{(v_{ij})^T x_{ij}}{||x_{ij}||}\frac{x_{ij}}{||x_{ij}||} \qquad (10)$$

where x_i and v_i are the position and velocity of vertex p_i, $x_{ij} = x_j - x_i$, $v_{ij} = v_j - v_i$, and k_{ij} and c_{ij} are the stiffness and damping coefficients of the spring connecting vertices p_i and p_j. The individual spring coefficients are determined based on a few manually selected global spring parameters shown in Table 1. These parameters are selected such that the skin becomes stiffer at locations closer to the bones such as around the elbow and ankle, and more compliant at other places to emulate the effect of thick soft tissue and muscle layers. To compute the spring coefficients of individual springs, K_{ss}, K_{mm}, and K_{dqm} are scaled by the size of the polygon that vertices belongs to, whereas K_{smb} is determined to be inversely proportional to the distance between the skin and bone vertices. In all cases, the damping coefficient is set to $d = \sqrt{k}/50$ for a connection with a spring coefficient of k. While these parameters are manually chosen, it is easy to find a set of values that yield reasonable simulation results.

Table 1: *Types of the springs and their global parameters.*

parameter	springs between vertices of	value
K_{ss}	skin–skin	10^4
K_{mm}	dynamic muscle–dynamic muscle	10^5
K_{dqm}	dynamic muscle–quasi-static muscle	10^2
K_{smb}	skin–dynamic muscle	10^7

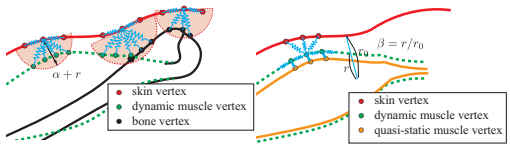

Figure 3: *Spring-damper connections between skin, muscle, and bone vertices*

We add all the forces from springs and dampers for each vertex in $\mathcal{P}^{s} \cup \mathcal{P}^{dm}$, and compute its acceleration by dividing by its mass that is computed from the total weight and the polygon size. We use the Velocity Verlet integration method [SABW82] to update the positions and velocities of the skin and muscle surface vertices. This method allows us to achieve high stability at no significant computational cost over the explicit Euler method. Although an implicit integration method [BW98] would allow a larger time step than explicit integration, that class of method is not suitable for our application because they add extra damping that diminishes the jiggling of the surface of the skin that we are modeling.

4. Results

The sample skin deformation data used for quasi-static muscle model identification are recorded with 400–450 reflective markers using 16 near-infrared Vicon MX-40 cameras at a rate of 120 fps [PH08]. The motion data used for the simulations are recorded with 60 reflective markers using the same motion capture system. We also record the contact force between the subject and the ground using two AMTI AccuSway PLUS force plates, each of which can measure the six-axis contact force and momentum at a rate of 1 kHz. Aurion ZeroWire system with 16 pairs of electrodes is used to capture EMG data of muscles beneath the electrodes at a rate of 5 kHz. The EMG data are processed by mean subtraction, rectification, and a Butterworth bandpass filter with a cut-off frequency of 10–1000 Hz. A high-speed video camera is also used for some of the motions to capture the dynamic skin deformation at 1 kHz (used for ground truth).

4.1. Evaluation of Identified Quasi-static Muscle Model

We first demonstrate the advantage of using musculoskeletal and muscle deformation models to obtain the underlying muscle shapes. As we mentioned in Section 3, we use the skin deformation data captured by markers densely placed on the skin to identify the muscle parameters. The distance between a marker and the closest point on the simulated skin surface indicates how well the muscle deformation model matches the actual skin deformation.

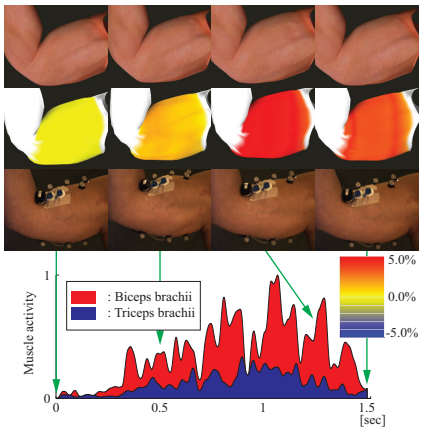

Figure 4: *Skin deformation simulation with muscle co-contraction.*

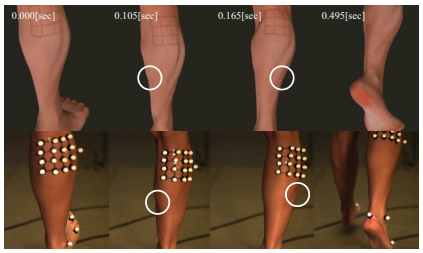

Figure 5: *Skin deformation simulated by our method (top) and corresponding images from high-speed video recording (bottom). The similar skin folds are realized especially at the white-circled place.*

We evaluate the quasi-static muscle deformation using two motion sequences: the slow jump motion used for identification and a slow walk motion for cross validation. The active deformation of the muscle is several millimeters even at the maximum muscle activity, which is much smaller than the deformation caused by the skeleton motion. The distance with deformation is 16.2 ± 2.3 mm (mean $\pm$ SD) for the slow jump and 18.6 ± 2.4 mm for th slow walk, while the distance without deformation is 18.4 ± 2.5 mm and 20.2 ± 2.5 mm respectively. This result shows that the distances are smaller with muscle deformation in both motions. Specifically, applying dynamic deformation to the quasi-static muscle deformation model results in larger improvement on average (approx. 2 mm) than the dynamic deformation used in [PH08] (approx. 1 mm). We also qualitatively compared our results with [PH08], and there is no significant visual difference between them.

4.2. Simulation Results

We now show simulated deformation of different parts of the skin for various motions to demonstrate our method. These motions are measured from a subject different from the one used for identifying the quasi-static muscle model using a standard marker set, force plates, EMG, and a high-speed camera recording for reference. The video clips of the simulated and recorded skin deformation are shown in the supplemental movie.

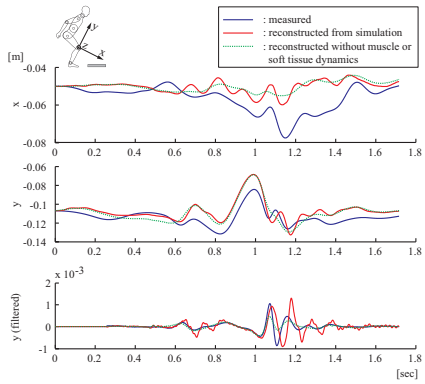

Figure 6: *Trajectories of the measured and simulated markers during the jump motion.*

Figure 4 shows a body building pose with tensing of the upper arm muscles. The top row represents the simulated skin deformation, the middle row represents the increase in the upper arm perimeter from the initial state, where the color changes from yellow to red as the perimeter increases, and the bottom row represents the corresponding snapshots from the high-speed video camera. The graph shows the normalized activities of the Biceps Brachii and Triceps Brachii obtained by post-processing the EMG data. The result shows that our method effectively simulates the bulging of the muscles during co-contraction, which is mainly detected by the EMG data because co-contraction of antagonistic muscles does not appear as joint motion. The skin jitters observed in the supplemental movie come from noise in the EMG signal, which remains even after the Butterworth bandpass filtering.

Figure 5 shows the simulation result for a running motion and Figure 6 represent the simulation results for a jump motion. In this motion capture session, we attached several markers in a grid pattern to quantitatively compare the actual and simulated skin deformations. Figure 6 plots the average trajectories of the 16 markers from the measured and simulated skin deformations. Each trajectory is represented in the local coordinate system fixed to the lower leg bone. The blue and red lines represent the measured and simulated trajectories of markers, which are on the softest part of the leg. The green dotted lines represent the marker trajectories that are simulated without muscle or soft tissue dynamics. The difference between the simulated skin deformation with muscle and soft tissue dynamics and the one without them is obvious. The third graph represents the y-direction trajectory that is post-processed by the Butterworth high-pass filter with a cut-off frequency of 100 Hz. This graph shows that the amplitude, frequency, and duration of the jiggles in the simulated skin deformation with muscle and soft tissue dynamics are similar to those in the measured motion, especially in the y direction just after the landing. This effect would not be realized without muscle or soft tissue dynamics.

The simulated skin deformation of hitting an object with his arm and the corresponding movie from the high-speed camera recording are shown in the supplemental movie. The high-speed camera shows the skin wrinkle around the elbow caused by the impact, which is also seen in our simulation. We include a parameter that

determines the average relative thickness of muscles with respect to soft tissue (β in Figure 3, right) to simulate different body types. The simulation result shows the skin deformation when this parameter is selected so that the model is 25 % less muscular in the supplemental movie. The amplitude of the skin jiggle becomes larger than that observed in the muscular model as expected.

5. Discussion

In this paper, we developed a new algorithm for simulating dynamic skin deformation in novel motion sequences based on an anatomical model of the musculoskeletal system and a passive dynamics model of soft tissue. This algorithm directly generates the skin deformation from skeletal motion data.

- The quasi-static muscle model allows us to compute the quasi-static muscle shape from muscle length and tension information for a wide range of motions. The resulting muscle shape is consistent with the dynamics of the motion because it is based on muscle pathway and tension data obtained by inverse kinematics and dynamics algorithms for a musculoskeletal model.
- The passive dynamics of the soft tissue effectively describes the interaction between the skin and internal bones and muscles. Our model can simulate skin deformations that depend on the underlying structure, such as different jiggling patterns when the skin hits the front side (tibia) and the calf side of the lower leg.
- This algorithm can simulate physiologically realistic skin deformations that are difficult to estimate only from standard motion capture data if EMG data are recorded along with the motion data. An example is muscle co-contraction, which cannot be estimated only from motion data because the activations of antagonistic pairs of muscles do not cause joint motion.

The simulation based methods tend to handle relatively static body parts and motions. The data-based methods are difficult to handle novel motions. Our method combines simulation-based and data-driven approaches: simulation allows us to obtain realistic results for a wide variety of motions, while a small set of data can be used to adapt the model to different body types.

We model the muscle and soft tissue dynamics with a mass-spring-damper system. This system is based on a realistic body shape created by a modeler, and the simple spindle-like muscle shape is only used to indicate how the detailed skin shape should deform. We chose a mass-spring-damper model because FEM would requires significantly higher computational cost and more parameter tuning than the mass-spring damper model even for a similar simulation resolution, though FEM shown in [WBD14] may be applied in principle. There are oscillation artifacts seen in our simulation that may caused by the explicit integration. Applying the implicit integration [BW98] may decrease these artifacts.

Our method has several limitations. The quasi-static muscle model parameter identification requires some frames of skin deformation data captured with a dense set of markers. As an alternative to measured skin deformation data, a modeler may provide the skin shapes at a few frames in a motion sequence. It is also possible that modern depth cameras could be used to provide this data. The other limitation is that we identified the quasi-static muscle model parameters assuming that the measured skin deformation data are not affected by the soft tissue dynamics. It may be possible to identify the two sets of parameters simultaneously using dynamic skin deformation data which might provide more accurate results.

References

[ASK*05] ANGUELOV D., SRINIVASAN P., KOLLER D., THRUN S., RODGERS J., DAVIS J.: SCAPE: Shape completion and animation of people. *ACM Transactions on Graphics 24* (2005), 408–416. 2

[BTS*05] BLEMKER S., TERAN J., SIFAKIS E., FEDKIW R., DELP S.: Fast 3d muscle simulations using a new quasistatic invertible finite-element algorithm. In *International Symposium on Computer Simulation in Biomechanics* (2005). 2

[BW98] BARAFF D., WITKIN A.: Large steps in cloth simulation. In *Proceedings of ACM SIGGRAPH 98* (1998), pp. 43–54. 4, 6

[DAA*07] DELP S., ANDERSON F., ARNOLD A., LOAN P., HABIB A., JOHN C., GUENDELMAN E., THELEN D.: OpenSim: Open-source software to create and analyze dynamic simulations of movement. *IEEE Transactions on Biomedical Engineering 54*, 11 (2007), 1940–1950. 2

[FLP14] FAN Y., LITVEN J., PAI D.: Active volumetric musculoskeletal systems. *ACM Transactions on Graphics (TOG) 33* (2014). 2

[Kar90] KARDEL T.: Niels Stensen's geometrical theory of muscle contraction (1667): A reappraisal. *The Journal of Biomechanics 23*, 10 (1990), 953–965. 3

[KMF*96] KOCH R., M.S. G., F.R. C., BÃIJREN D., FANKHAUSER G., PARISH Y.: Simulating facial surgery using finite element models. In *Proceedings of ACM SIGGRAPH 96* (1996), pp. 421–428. 2

[LAR*14] LEWIS J., ANJYO K., RHEE T., ZHANG M., PIGHIN F., DENG Z.: Practice and theory of blendshape facial models. In *Proceedings of Eurographics 2014 - State of the Art Reports* (2014). 1, 2

[LGK*12] LEE D., GLUECK M., KHAN A., FIUME E., JACKSON K.: Modeling and simulation of skeletal muscle for computer graphics: A survey. *ACM Transactions on Graphics 28* (2012). 2

[LWP80] LUH J., WALKER M., PAUL R.: On-line Computational Scheme for Mechanical Manipulators. *ASME Journal on Dynamic Systems, Measurment and Control 104* (1980), 69–76. 3

[MTMN14] MURAI A., TAKEICHI K., MIYATAKE T., NAKAMURA Y.: Musculoskeletal modeling and physiological validation. *2014 IEEE Workshop on Advanced Robotics and its Social Impacts (ARSO)* (2014), 108–113. 1, 2, 3

[PH08] PARK S., HODGINS J.: Data-driven modeling of skin and muscle deformation. *ACM Transactions on Graphics 27*, 3 (2008), 96:1–96:6. 1, 2, 4, 5

[SABW82] SWOPE W., ANDERSEN H., BERENS P., WILSON K.: A computer simulation method for the calculation of equilibrium constants for the formation of physical clusters of molecules: Application to small water clusters. *The Journal of Chemical Physics 76* (1982). 4

[SLST14] SI W., LEE S., SIFAKIS E., TERZOPOULOS D.: Realistic biomechanical simulation and control of human swimming. *ACM Transactions on Graphics (TOG) 34* (2014). 1

[WBD14] WEBB J., BLEMKER S., DELP S.: 3d finite element models of shoulder muscles for computing lines of actions and moment arms. *Comput Methods Biomech Biomed Engin. 17* (2014), 829–837. 6

[YFN05] YAMANE K., FUJITA Y., NAKAMURA Y.: Estimation of physically and physiologically valid somatosensory information. In *Proceedings of IEEE International Conference on Robotics and Automation* (2005), pp. 2635–2641. 3

[ZCCD04] ZORDAN V., CELLY B., CHIU B., DILORENZO P.: Breathe easy: model and control of simulated respiration for animation. In *Proceedings of ACM SIGGRAPH / Eurographics Symposium on Computer Animation* (2004), pp. 29–37. 2